

An additive framework for kirigami design

Levi H. Dudte[†], Gary P. T. Choi^{1,†}, Kaitlyn P. Becker², L. Mahadevan^{2,3,*}

¹Department of Mathematics, Massachusetts Institute of Technology, Cambridge, MA, USA

²School of Engineering and Applied Sciences, Harvard University, Cambridge, MA, USA

³Departments of Physics, and Organismic and Evolutionary Biology, Harvard University, Cambridge, MA, USA

[†]L.H.D. and G.P.T.C. contributed equally to this work.

*To whom correspondence should be addressed; E-mail: lmahadev@g.harvard.edu

Abstract

We present an additive approach for the inverse design of kirigami-based mechanical metamaterials by focusing on the design of the negative spaces instead of the kirigami tiles. By considering each negative space as a four-bar linkage, we discover a simple recursive relationship between adjacent linkages, yielding an efficient method for creating kirigami patterns. This shift in perspective allows us to solve the kirigami design problem using elementary linear algebra, with compatibility, reconfigurability and rigid-deployability encoded into a design matrix. The resulting linear design strategy circumvents the solution of non-convex global optimization problems and allows us to control the degrees of freedom in the deployment angle field, linkage offsets and boundary conditions. We demonstrate this by creating a large variety of rigid-deployable, compact reconfigurable kirigami patterns. We then realize our kirigami designs physically using two new simple but effective fabrication strategies with very different materials. All together, our additive approaches pave a new way for mechanical metamaterial design and fabrication based on paper-based (ori/kiri-gami) art forms.

1 Introduction

Kirigami, the traditional papercrafting art, has inspired the design of shape-shifting structures in science and engineering in recent years [1–6]. There have been numerous studies exploring different kirigami-based deployable structures [7–22] and generalizing their geometry and topology [23–28], with a focus that is primarily on the forward problem. This has been complemented by an inverse design framework for producing compact reconfigurable and rigid-deployable kirigami patterns [29] admitting multiple closed and compact contracted configurations which do not require tile deformations to transform from one to another. Specifically, the framework involves setting up a global constrained optimization problem that encodes the compact reconfigurability and rigid-deployability as geometric constraints in terms of the angles and lengths of the kirigami tiles. While such an approach is capable of producing compact reconfigurable and rigid-deployable kirigami patterns and mechanisms with different shape changes, the process of finding a solution to the nonlinear global constrained optimization problem for large patterns is both computationally difficult and hard to control. Moreover, we do not completely understand the underlying degrees of freedom in the design space. A step in simplifying this process was taken in [30] by creating rigid-deployable quad kirigami tessellations with different topologies via solving a matrix equation for the node coordinates of all tiles in a closed and compact configuration.

Recently, we introduced a change in the perspective in the design of origami-based mechanical metamaterials [31] by switching from a global optimization perspective to a locally constrained additive process. This allowed us to derive a nonlinear marching algorithm that characterizes the design space of quad origami, and provides a simple and effective algorithm for the origamization of any surface. Here, we show kirigami also

lends itself to a similar but even simpler additive approach that identifies and exploits a *linear* marching construction to connect local growth rules to global form for the design of quad kirigami in any contracted or deployed space. Furthermore, we show that we can control the flexibility of encoding contractibility, compact reconfigurability and rigid-deployability in a simple design matrix characterized by a combination of certain edge length and angle parameters. This significantly simplifies the process of designing kirigami patterns as matrix multiplications. Our approach of decoupling the length field, angle field and the boundary node constraints allows us to systematically analyze the degrees of freedom in the design space of different types of quad kirigami tessellations.

2 Additive design framework

Analogous to our additive origami design approach [31], we tackle the kirigami design problem by working our way up a ladder of hierarchical complexity, beginning with the smallest building block, a single four-bar linkage representing the negative space of a unit cell of four quads, before moving on to strips of linkages and finally linkage arrays. At each level, our strategy will be to describe a marching geometric construction, the *forward* process, which can be cast as matrix multiplication, allowing us then to convert the marching algorithm into a flexible and intuitive design framework using linear *inverse* design techniques.

In Fig. 1 we show an overview of the marching construction for linear quad kirigami design. The key idea is to identify the constraints in the negative spaces in a deployed configuration, and use them to form a design matrix which is nonlinearly dependent on the deployment angles and edge lengths. However, once the matrix is determined, the coordinates of all nodes can be obtained by a simple matrix multiplication step, yielding a linear design method of quad kirigami.

2.1 Linkage design

To simplify our discussion, we start by considering the design of a negative space surrounded by four quads represented as a parallelogram four-bar linkage in \mathbb{R}^2 given by $\mathbf{x}_k = (x_k, y_k)$, $k \in \{0, 1, 2, 3\}$ with the *deployment angle* $\phi = \angle(\mathbf{x}_1, \mathbf{x}_0, \mathbf{x}_3)$ at \mathbf{x}_0 (Fig. 1A). We parameterize its construction according to

$$\begin{bmatrix} I - Q & Q \\ -Q & I + Q \end{bmatrix} \begin{bmatrix} \mathbf{x}_0 \\ \mathbf{x}_3 \end{bmatrix} = \begin{bmatrix} \mathbf{x}_1 \\ \mathbf{x}_2 \end{bmatrix}, \quad (1)$$

where $Q = (1 + \epsilon)R(-\phi)$ is a scaled rotation matrix with ϵ being a scalar which we refer to as the *offset*, $I = \begin{bmatrix} 1 & 0 \\ 0 & 1 \end{bmatrix}$ and $R(-\phi) = \begin{bmatrix} \cos \phi & \sin \phi \\ -\sin \phi & \cos \phi \end{bmatrix}$ are the identity and rotation matrices in \mathbb{R}^2 , respectively, and

$\begin{bmatrix} \mathbf{x}_i \\ \mathbf{x}_j \end{bmatrix} = \begin{bmatrix} x_i \\ y_i \\ x_j \\ y_j \end{bmatrix}$ is a column vector of coordinates of two points in the parallelogram. Extending (1) yields

an 8×4 linkage design matrix D that takes two points \mathbf{x}_0 and \mathbf{x}_3 (the red nodes in Fig. 1A) as input and returns as output four points $\mathbf{x}_k = (x_k, y_k)$, $k \in \{0, 1, 2, 3\}$ to form the parallelogram:

$$D \begin{bmatrix} \mathbf{x}_0 \\ \mathbf{x}_3 \end{bmatrix} = \begin{bmatrix} I & 0 \\ I - Q & Q \\ -Q & I + Q \\ 0 & I \end{bmatrix} \begin{bmatrix} \mathbf{x}_0 \\ \mathbf{x}_3 \end{bmatrix} = \begin{bmatrix} \mathbf{x}_0 \\ \mathbf{x}_1 \\ \mathbf{x}_2 \\ \mathbf{x}_3 \end{bmatrix}. \quad (2)$$

Our choice of parameterization measures a kind of eccentricity of the parallelogram (its departure from a rhombus) by the offset ϵ and forms a counter-clockwise polar coordinate system ($r = 1 + \epsilon$, $-\phi$) centered at \mathbf{x}_0 with $\phi = 0$ in the direction of $\mathbf{x}_3 - \mathbf{x}_0$. When $\epsilon = 0$ the parallelogram is a rhombus and when $\epsilon = -1$ the parallelogram degenerates to two equal collinear line segments with $\mathbf{x}_0 = \mathbf{x}_1$ and $\mathbf{x}_2 = \mathbf{x}_3$. Otherwise, so

long as $\phi \neq 0, \pi$ the generated points \mathbf{x} form a parallelogram in \mathbb{R}^2 for all values of ϵ . The points are ordered counter-clockwise when $\phi < \pi$, clockwise when $\phi > \pi$ and are collinear when $\phi = \pi$. Holding ϵ constant keeps each edge length in the parallelogram constant and varying ϕ casts the parallelogram as a four-bar linkage, giving its one-dimensional deployment path. During deployment, two opposite interior angles in the linkage each measure ϕ and the other two each measure $\pi - \phi$ (see SI Section S1A for more details).

2.2 Linkage strips and linkage arrays

Now we will analyze the design of two parallelogram four-bar linkages having one common point and generalize this system to strips and arrays of connected linkages. Consider the first two adjacent linkages in the first row of Fig. 1B comprised of seven total nodes so that one node is shared by both. The linkage points can be labeled $\mathbf{x}_{j,k}^0$ where $j \in \{0, 1\}$ is the linkage index, $k \in \{0, 1, 2, 3\}$ is the point in linkage index and $\mathbf{x}_{0,2}^0 = \mathbf{x}_{1,0}^0$ denotes the shared node. The linkages each have their own deployment angles ϕ_j^0 and offsets ϵ_j^0 . It can be observed that once $\mathbf{x}_{0,0}^0, \mathbf{x}_{0,3}^0, \phi_0^0$ and ϵ_0^0 in the first linkage are given, $\mathbf{x}_{0,1}^0, \mathbf{x}_{0,2}^0$ are uniquely determined. In particular, as $\mathbf{x}_{0,2}^0$ is already determined, it suffices to prescribe $\mathbf{x}_{1,3}^0, \phi_1^0$ and ϵ_1^0 to uniquely determine all points in the second linkage.

We can apply this insight to a more complex linkage strip of n linkages $\mathbf{x}_{j,k}^0$ as shown in the first row of Fig. 1B, where $j \in \{0, \dots, n-1\}$ is the linkage index, $k \in \{0, 1, 2, 3\}$ is a point in linkage index and $\mathbf{x}_{j,2}^0 = \mathbf{x}_{j+1,0}^0$ denotes a shared node. In other words, we can obtain a series of linkage design matrices $D_0^0, D_1^0, \dots, D_{n-1}^0$ that encode the recursive dependency of the nodes on the previously determined nodes via dynamic programming (see SI Section S1B). Once the relationship in a linkage strip is determined, we can proceed to consider the relationship in a linkage array consisting of multiple linkage strips analogously, noticing that the (i, j) -th linkage in the array is dependent of all linkages (\tilde{i}, \tilde{j}) with $\tilde{i} \leq i$ and $\tilde{j} \leq j$ recursively (see SI Section S1C for more details). More specifically, the entire linkage array is dependent of the seed nodes $\{\mathbf{x}_{0,0}^0, \mathbf{x}_{0,3}^0, \mathbf{x}_{1,3}^0, \dots, \mathbf{x}_{n-1,3}^0, \mathbf{x}_{0,0}^1, \mathbf{x}_{0,0}^2, \dots, \mathbf{x}_{0,0}^{m-1}\}$ consisting of all the left boundary points and all the top boundary points in the linkage array (the red nodes in Fig. 1B), the deployment angle field $\{\phi_j^i\}$, and the offset field $\{\epsilon_j^i\}$. We remark that the deployment angles $\{\phi_j^i\}$ have to satisfy certain additional conditions in order to yield a kirigami pattern with different physical properties such as contractibility and compact reconfigurability, which will be discussed later.

2.3 Global linear inverse design via matrix operations

Putting all of these pieces together, for an array of $m \times n$ planar parallelogram four-bar linkages with nodes $\{\mathbf{x}_{j,k}^i, i \in \{0, 1, \dots, m-1\}, j \in \{0, 1, \dots, n-1\}, k \in \{0, 1, 2, 3\}\}$, we obtain a full linkage array design matrix M of size $(4mn + 2m + 2n) \times (2m + 2n)$. In particular, we have

$$M \begin{bmatrix} \mathbf{x}_{0,0}^0 \\ \mathbf{x}_{0,3}^0 \\ \mathbf{x}_{1,3}^0 \\ \vdots \\ \mathbf{x}_{n-1,3}^0 \\ \mathbf{x}_{0,0}^1 \\ \mathbf{x}_{0,0}^2 \\ \vdots \\ \mathbf{x}_{0,0}^{m-1} \end{bmatrix} = \begin{bmatrix} D_0^0 \\ D_1^0 \\ \vdots \\ D_{n-1}^0 \\ D_0^1 \\ D_1^1 \\ \vdots \\ D_{n-2}^{m-1} \\ D_{n-1}^{m-1} \end{bmatrix} \begin{bmatrix} \mathbf{x}_{0,0}^0 \\ \mathbf{x}_{0,3}^0 \\ \mathbf{x}_{1,3}^0 \\ \vdots \\ \mathbf{x}_{n-1,3}^0 \\ \mathbf{x}_{0,0}^1 \\ \mathbf{x}_{0,0}^2 \\ \vdots \\ \mathbf{x}_{0,0}^{m-1} \end{bmatrix} = \begin{bmatrix} \mathbf{x}_{0,0}^0 \\ \mathbf{x}_{0,1}^0 \\ \mathbf{x}_{0,2}^0 \\ \mathbf{x}_{0,3}^0 \\ \mathbf{x}_{1,1}^0 \\ \mathbf{x}_{1,2}^0 \\ \mathbf{x}_{1,3}^0 \\ \vdots \\ \mathbf{x}_{n-1,1}^{m-1} \\ \mathbf{x}_{n-1,2}^{m-1} \\ \mathbf{x}_{n-1,3}^{m-1} \end{bmatrix} \quad (3)$$

with

$$M = \begin{bmatrix} D_0^0 \\ D_1^0 \\ \vdots \\ D_{n-1}^0 \\ D_0^1 \\ D_1^1 \\ \vdots \\ D_{n-2}^{m-1} \\ D_{n-1}^{m-1} \end{bmatrix} = \begin{bmatrix} I & 0 & 0 & 0 \\ G_{0,0}^{0,0} & G_{0,0}^{0,1} & 0 & 0 \\ G_{0,0}^{1,0} & G_{0,0}^{1,1} & 0 & 0 \\ 0 & I & 0 & 0 \\ G_{0,1}^{0,0} G_{0,0}^{0,0} & G_{0,1}^{0,0} G_{0,0}^{0,1} & G_{0,1}^{0,1} & 0 \\ G_{0,1}^{1,0} G_{0,0}^{1,0} & G_{0,1}^{1,0} G_{0,0}^{1,1} & G_{0,1}^{1,1} & 0 \\ 0 & 0 & I & 0 \\ G_{0,2}^{0,0} G_{0,1}^{1,0} G_{0,0}^{1,0} & G_{0,2}^{0,0} G_{0,1}^{1,0} G_{0,0}^{1,1} & G_{0,2}^{0,0} G_{0,1}^{1,1} & G_{0,2}^{0,1} \\ G_{0,2}^{1,0} G_{0,1}^{1,0} G_{0,0}^{1,0} & G_{0,2}^{1,0} G_{0,1}^{1,0} G_{0,0}^{1,1} & G_{0,2}^{1,0} G_{0,1}^{1,1} & G_{0,2}^{1,1} \\ 0 & 0 & 0 & I \\ \vdots & \vdots & \vdots & \ddots \end{bmatrix}, \quad (4)$$

where D_j^i are the linkage design matrices which can be expressed in terms of the following generator matrices using dynamic programming (see SI Section S1C for more details):

$$\begin{bmatrix} G_{i,j}^{0,0} & G_{i,j}^{0,1} \\ G_{i,j}^{1,0} & G_{i,j}^{1,1} \end{bmatrix} = \begin{bmatrix} I - (1 + \epsilon_j^i)R(-\phi_j^i) & (1 + \epsilon_j^i)R(-\phi_j^i) \\ -(1 + \epsilon_j^i)R(-\phi_j^i) & I + (1 + \epsilon_j^i)R(-\phi_j^i) \end{bmatrix}. \quad (5)$$

The sparsity of the matrix M forms a simple pattern (Fig. 1C): after the first block row, each of the next n set of three block rows has entries in a new block column unoccupied by all block rows above it in the matrix. For example, the fifth, sixth and seventh block rows in (3) contain $G_{0,1}^{0,1}$, $G_{0,1}^{1,1}$ and I , respectively, as entries in the third block column, which contains only zero entries in the block rows above the fifth. After that, each of the next $(m-1)$ set of $(n+1)$ block rows has entries in a new block column unoccupied by all block rows above it in the matrix. This makes it easy to observe that a submatrix M^{sub} of M comprised of any two block rows from the first four block rows, and one block row from each of the subsequent sets of block rows (i.e. with a total of $2 + (n-1) + (m-1) = m+n$ block rows) will be a $(2m+2n) \times (2m+2n)$ square matrix with full rank and hence invertible.

This observation suggests a linear design strategy for quad kirigami patterns. To create a quad kirigami pattern consisting of $(m+1) \times (n+1)$ quads, we need to fully determine an array of $m \times n$ planar parallelogram four-bar linkages representing all negative spaces. This linear inverse design process for the linkage array is summarized as follows:

1. Assemble the full linkage array design matrix M (Fig. 1C, first panel). Note that this requires choosing the deployment angle ϕ_j^i and offset ϵ_j^i for each linkage (i, j) , which will be discussed in detail in the next section.
2. Choose a subset of $(m+n)$ points $\{\tilde{\mathbf{x}}_0, \tilde{\mathbf{x}}_1, \dots, \tilde{\mathbf{x}}_{m+n-1}\}$ in the linkage array such that the corresponding block rows of them in M form a $(2m+2n) \times (2m+2n)$ matrix M^{sub} with full rank (Fig. 1C, second panel). The coordinates of these points can be prescribed directly by the designer as boundary conditions. We can then use them to find the seed nodes in (3):

$$\begin{bmatrix} \mathbf{x}_{0,0}^0 \\ \mathbf{x}_{0,3}^0 \\ \mathbf{x}_{1,3}^0 \\ \vdots \\ \mathbf{x}_{n-1,3}^0 \\ \mathbf{x}_{0,0}^1 \\ \mathbf{x}_{0,0}^2 \\ \vdots \\ \mathbf{x}_{0,0}^{m-1} \end{bmatrix} = (M^{\text{sub}})^{-1} \begin{bmatrix} \tilde{\mathbf{x}}_0 \\ \tilde{\mathbf{x}}_1 \\ \tilde{\mathbf{x}}_2 \\ \vdots \\ \tilde{\mathbf{x}}_{m+n-2} \\ \tilde{\mathbf{x}}_{m+n-1} \end{bmatrix}. \quad (6)$$

In particular, if we simply choose $\{\tilde{\mathbf{x}}_0, \tilde{\mathbf{x}}_1, \dots, \tilde{\mathbf{x}}_{m+n-1}\}$ to be the seed nodes (i.e. all the top and left boundary points in the linkage array), then M^{sub} is simply the $(2m+2n) \times (2m+2n)$ identity matrix.

3. Calculate the full linkage array by a direct matrix multiplication using (6) together with (3) (Fig. 1C, third panel).
4. For the boundary nodes of the $(m+1) \times (n+1)$ kirigami pattern that are not included in the linkage array, one can determine their coordinates uniquely using the linkage array obtained in the last step together with four prescribed corner positions and a set of desired *boundary offsets* (see SI Section S1D for details).

2.4 Choices of the deployment angles and the offsets

As discussed previously, the full design matrix M is determined by the deployment angles and offsets of every four-bar linkage negative space. Here, the angles $\{\phi_j^i\}$ in the negative spaces are related by certain local angle rules. Depending on the desired properties of the resulting kirigami pattern, the degrees of freedom (DOFs) in them will be different.

2.4.1 Contractibility

For a quad kirigami pattern to be contractible, each unit cell consisting of four adjacent tiles has to satisfy an edge length constraint and an angle sum constraint [25]. Specifically, suppose the four edges of a negative space are with length a, b, c, d and the four angles of the tiles are $\alpha, \beta, \gamma, \delta$ as shown in Fig. 2A, the following conditions must be satisfied:

$$a + d = b + c, \quad (7)$$

$$\alpha + \beta + \gamma + \delta = 2\pi. \quad (8)$$

In our formulation of the parallelogram four-bar linkages, we have $a = c$ and $b = d$ and hence the edge length constraint in (7) is automatically satisfied (note that here we do not require the four angles to meet at a common point as we have the flexibility to change the offset). Now, we rewrite the angle sum constraint using the deployment angles of the (i, j) -th four-bar linkage and its adjacent linkages. As shown in Fig. 2A, we have

$$\alpha + \delta + (\pi - \phi_j^i) + (\pi - \phi_j^{i+1}) = 2\pi, \quad (9)$$

$$\beta + \gamma + (\pi - \phi_j^i) + (\pi - \phi_j^{i-1}) = 2\pi. \quad (10)$$

Therefore, the angle sum constraint in (8) can be rewritten as

$$\phi_j^{i-1} + 2\phi_j^i + \phi_j^{i+1} = 2\pi. \quad (11)$$

As the deployment direction of adjacent linkages is alternating, for the entire $m \times n$ linkage array, we have

$$\begin{cases} \phi_j^{i-1} + 2\phi_j^i + \phi_j^{i+1} = 2\pi & \text{if } i+j \text{ is odd,} \\ \phi_{j-1}^i + 2\phi_j^i + \phi_{j+1}^i = 2\pi & \text{if } i+j \text{ is even,} \end{cases} \quad (12)$$

where $i = 0, \dots, m-1$ and $j = 0, \dots, n-1$. Note that some of the above equations involve ghost points with out-of-range indices, namely $\phi_j^{-1}, \phi_j^m, \phi_{-1}^i, \phi_n^i$, which are free variables that can be prescribed arbitrarily. Once the values of them have been prescribed, (12) has full rank and gives a unique set of ϕ_j^i values for all i, j . In other words, the number of DOFs in the space of deployment angles of a contractible $m \times n$ linkage array is exactly $2(m+n)$.

Fig. 2B (left) shows an example deployed pattern obtained by the linear inverse design approach, where the offset field $\{\epsilon_j^i\}$ is set to be uniformly 0 in the design matrix and the deployment angle field $\{\phi_j^i\}$ is set arbitrarily. The coordinates of certain linkage array boundary nodes (red) are prescribed as the boundary

conditions for solving the seed coordinates to get the linkage array, and then the four corners of the kirigami pattern (blue) are further prescribed to uniquely determine the remaining boundary nodes of the resulting kirigami pattern. It can be observed that the resulting pattern is non-contractible, with the two maximally contracted states containing holes. By contrast, Fig. 2B (middle) shows an example pattern obtained by the linear inverse design approach with the contractibility constraint in (12) enforced in the design matrix and all other parameters being the same as the previous example. This time, we can see that the resulting pattern admits a closed and compact contracted configuration.

2.4.2 Reconfigurability

For a kirigami pattern to be compact reconfigurable, i.e. admitting two closed and compact contracted states, it should satisfy the above contractibility constraints as well as a set of dual edge length constraints $a + b = c + d$ and dual angle sum constraints [29]. In the formulation of the parallelogram four-bar linkages, the dual edge length constraint is again automatically satisfied as we have $a = c$ and $b = d$ in Fig. 2A. Note that the dual angle sum constraint at every four-bar linkage (i, j) is simply the dual case in (12). In other words, for a compact reconfigurable quad kirigami pattern, the corresponding linkage array should satisfy

$$\begin{cases} \phi_j^{i-1} + 2\phi_j^i + \phi_j^{i+1} = 2\pi, \\ \phi_{j-1}^i + 2\phi_j^i + \phi_{j+1}^i = 2\pi, \end{cases} \quad (13)$$

for every pair of $(i, j) \in \{0, 1, \dots, m-1\} \times \{0, 1, \dots, n-1\}$. This implies that

$$\begin{cases} \phi_j^i = \phi & \text{if } i + j \text{ is even,} \\ \phi_j^i = \pi - \phi & \text{if } i + j \text{ is odd,} \end{cases} \quad (14)$$

where ϕ is the deployment angle of the first linkage in the array. In other words, there is exactly 1 DOF in the entire deployment angle field $\{\phi_j^i\}$. In particular, this DOF captures the state of deployment of the pattern. Note that this agrees with the observation in our recent study [29].

Fig. 2B (right) shows an example pattern obtained by solving the matrix equation with (13) enforced, where the boundary condition is given by the same set of boundary linkage vertices (red) and corner vertices (blue) as in the previous examples. It can be observed that the resulting pattern admits multiple closed and compact contracted configurations. We also note that due to the difference in the flexibility of the angle field, the resulting patterns in Fig. 2B are significantly different in shape.

2.4.3 Rigid-deployability

In our recent work [29], we derived the conditions on edge lengths and angles of kirigami tiles for achieving rigid-deployability. In the current additive design framework, the rigid-deployability depends on the geometry of the parallelogram four-bar linkages as well as the contractibility and compact reconfigurability discussed above.

For any non-contractible pattern created by our approach such as the example in Fig. 2B (left), the pattern is always rigid-deployable in between the two maximally contracted states as the parallelogram four-bar linkages can deploy and contract without any geometrical frustration.

For any contractible pattern created by our approach such as Fig. 2B (middle), the rigid-deployability near the fully contracted state depends on the geometry of the four-bar linkages. If all four-bar linkages are not rhombi, they will always form a straight line at the fully contracted state and hence the kirigami pattern is rigid-deployable in between the fully contracted state and the second maximally contracted state. However, if some of the four-bar linkages are rhombi, they do not necessarily form a straight line at the fully contracted state and hence the pattern will generally be not rigid-deployable unless certain extra angle constraints are enforced as described in [29]. In fact, it can be observed that the contractible kirigami pattern in Fig. 2B

(middle) contains negative spaces that do not form a straight line in the fully contracted state, which indicates that the pattern is not rigid-deployable.

For any compact reconfigurable pattern created by our approach such as Fig. 2B (right), the parallelogram four-bar linkage assumption together with the angle constraint in (14) will automatically satisfy the conditions for rigid-deployability in [29]. Therefore, the compact reconfigurable kirigami patterns created by our approach are always rigid-deployable.

2.4.4 Offset field

Note that the offsets $\{\epsilon_j^i\}$ of all linkages can be chosen independently as long as they do not lead to degeneracies or self-intersections. As shown in Fig. 2C, different choices of the offsets can be used for creating a compact reconfigurable, rigid-deployable heart structure. Setting a uniform offset $\epsilon_j^i = 0$ at all linkages leads to a more regular and symmetric second contracted state (top row), while setting a large offset $\epsilon_j^i \gg 1$ for one particular linkage creates a more irregular shape locally (middle row). Setting a large offset at multiple linkages produces a much more irregular second contracted state (bottom row). See SI Section S4 for more example choices of the offsets and their effects.

3 Linear and nonlinear inverse design

With the proposed additive design approach, we now have full control of the design of quad kirigami patterns. In particular, we have characterized the design space of contractible quad kirigami patterns as well as that of rigid-deployable, compact reconfigurable quad kirigami patterns: We can inverse design all such patterns by prescribing the desired interior properties via the deployment angle and offset fields in the design matrix, specifying certain boundary conditions, solving a matrix equation to find the corresponding seed coordinates, and finally using a direct matrix multiplication to obtain the resulting patterns. Moreover, this linear design approach suggests that it is indeed possible to design kirigami patterns that match any prescribed shape at any prescribed stage of deployment, as the deployment angle field and the boundary conditions are set in two separate steps. To illustrate this idea, in Fig. 3A we design two rigid-deployable, compact reconfigurable kirigami patterns that deploy to a circle at the deployed state with $\phi = \pi/2$ (i.e. all negative spaces are rectangular) and a trapezium at the deployed state with $\phi = \pi/4$ (i.e. all negative spaces are parallelogram with the acute angle being $\pi/4$) respectively, from which it can be observed that we have precise control of the shape matching and the deployment angle (see SI Section S4 for more results).

A natural next question is whether it is possible to match multiple target shapes at multiple stages of deployment. Since the boundary conditions have already been used for enforcing the shape of the pattern at a certain stage, we cannot use them to control the shape at another state. Nevertheless, there are still DOFs in the angles and edge lengths in setting the design matrix. This suggests a nonlinear inverse kirigami design approach for approximating multiple prescribed shapes at multiple states: Given a certain nonlinear objective function that quantifies the optimality of a kirigami pattern, we can search for an optimal pattern effectively by solving the optimization problem over the remaining set of the design parameters. For instance, we can solve for a target second contracted shape by fixing the deployment angle as $\phi = \pi$ and optimizing the offset parameters $\{\epsilon_j^i\}$ (see SI Section S2 and S3 for more details). Fig. 3B shows various nonlinear inverse design results of rigid-deployable, compact reconfigurable kirigami patterns that morph from a closed and compact square to a target second closed and compact shape. Analogous to our recent work [29], our method is capable of producing a square-to-circle shape change. Moreover, we can achieve a lot more different target shapes with different curvature properties at the second contracted state (see SI Section S4 for more results). The larger variety of patterns we can obtain is attributed to the simplified parameter space in the novel additive design formulation.

With the above linear and nonlinear inverse design results, one may ask about the limit of the shapes achievable by introducing cuts on a square. As the design space of the rigid-deployable, compact reconfigurable quad kirigami patterns is fully characterized by our framework, we can easily generate a large number of such patterns by setting the design matrix parameters randomly and perform a statistical analysis. Here we fix the linkage array size as $m \times n = 10 \times 10$ and generate 10000 kirigami patterns on a unit square with random offsets $\{\epsilon_j^i\}$. More specifically, for each trial, the boundary nodes of the pattern are enforced to lie on a unit square with uniform spacing and the deployment angle ϕ is set to be 0. The offset ϵ_j^i of each linkage (i, j) is randomly sampled within $-0.99 \leq \epsilon_j^i \leq 0.99$ to ensure that there is no degeneracy or self-intersection. We then use the proposed method with the above parameters to obtain a rigid-deployable, compact reconfigurable square kirigami pattern, and then assess the geometric properties of its fully deployed configuration ($\phi = \pi/2$) and its second contracted configuration ($\phi = \pi$) such as diagonal ratio and area as functions of ϕ (see SI Section S5 for more details). Specifically, by considering the ratio r_d between the two diagonal lengths of a structure at different states, we can assess the shear of the overall shape as ϕ increases. As shown in Fig. 3C, the diagonal ratio at the fully deployed state ($r_d(\pi/2)$) and that at the second contracted state ($r_d(\pi)$) forms a highly linear relationship. It is also noteworthy that the reconfigured diagonal ratio is always larger than the deployed diagonal ratio, which suggests a natural limitation on the possible shape change achievable throughout the deployment. As for the overall area of the pattern r_a , it can be shown that the maximum deployed area of the pattern is always achieved at $\phi = \pi/2$. Comparing the diagonal ratio and the maximum deployed area of the random patterns, we find that these quantities are positively correlated. One can also consider other quantities such as the side length ratio r_l and study the relationship between them (see SI Section S5). We remark that as the proposed design framework only involves simple matrix operations, the generation and analysis of each pattern are highly efficient and take less than 0.5 seconds.

4 Physical model fabrication

It is natural to ask how one can realize the rigid-deployable, compact reconfigurable kirigami patterns obtained by the additive design framework. In particular, a careful treatment of the hinges in between the tiles is important to enable compact reconfigurability of the patterns in practice. While it is possible to use tape joints to connect the tiles as illustrated in our prior work [29], the fabrication is time-consuming and the hinges are likely to fatigue and break. To circumvent both issues, we propose two new fabrication techniques for manufacturing robust kirigami models.

4.1 3D printing-based approach

To create a physical model with rigid tiles, we can start by 3D printing the kirigami tiles with hollow slots where fatigue-resistant fabric hinges can be glued in place (Fig. 4A). The tiles can be printed individually and arranged for maximal packing density on a printer bed but we chose to print the tiles in a deployed configuration with temporary trusses to guide tile placement and facilitate hinge insertion. After the hinges were installed, the trusses were then trimmed away. Using this approach, we can achieve rigid-deployable, compact reconfigurable kirigami structures with higher out of plane bending stiffness easily, as compared to the soft kirigami sheets described below. For illustration, we fabricate the heart pattern obtained by linear inverse design using this approach (Fig. 4B). It can be observed that the deployment of the physical model matches that of the computational result very well (see SI Section S6 for more details of the fabrication technique).

4.2 Casting and molding approach

Alternatively, we can create soft kirigami sheets using a molding approach (Fig. 4C). We start by producing 2.5D laser cut molds based on a deployed configuration of the kirigami patterns obtained by our framework, adding fabric at the hinges. We then fill the mold and encase the fabric hinges with a silicone rubber to

produce a physical model. This approach facilitates fabrication of large arrays and allows us to minimize the size and stiffness of the hinges. For illustration, we fabricate the square-to-circle pattern obtained by nonlinear inverse design (Fig. 4D) and see that the deployment of the physical models matches that of the computational results very well (see SI Section S6 for more details).

5 Conclusions

In this work, we have presented a novel additive perspective for kirigami design. In particular, the parallelogram four-bar linkage construction allows us to easily parameterize each negative space by two parameters ϕ and ϵ and establish a design matrix by considering the relationship between adjacent linkages, thereby leading to a simple method for designing quad kirigami patterns via matrix operations. Our method decouples the fields of deployment angles and lengths of the cut patterns and hence gives a better understanding of the design space of quad kirigami. From the structure of the design matrix, one can also precisely identify the DOFs in the control of the overall pattern shape from the viewpoint of matrix rank. Altogether, our proposed formulation effectively characterizes the design space of quad kirigami patterns and hence can be applied to many design problems in science and engineering. Our combination of 3D printing and casting approaches provide a relatively inexpensive and efficient way of manufacturing kirigami models with fatigue-resistant hinges. A possible future direction is to extend the additive design formulation for more general kirigami patterns with non-parallelogram negative spaces [25].

References

- [1] A. Lamoureux, K. Lee, M. Shlian, S. R. Forrest, and M. Shtein, “Dynamic kirigami structures for integrated solar tracking,” *Nat. Commun.*, vol. 6, no. 1, pp. 1–6, 2015.
- [2] R. Zhao, S. Lin, H. Yuk, and X. Zhao, “Kirigami enhances film adhesion,” *Soft Matter*, vol. 14, no. 13, pp. 2515–2525, 2018.
- [3] A. Rafsanjani, Y. Zhang, B. Liu, S. M. Rubinstein, and K. Bertoldi, “Kirigami skins make a simple soft actuator crawl,” *Sci. Robot.*, vol. 3, no. 15, p. eaar7555, 2018.
- [4] S. Babaei, S. Pajovic, A. Rafsanjani, Y. Shi, K. Bertoldi, and G. Traverso, “Bioinspired kirigami metasurfaces as assistive shoe grips,” *Nat. Biomed. Eng.*, vol. 4, no. 8, pp. 778–786, 2020.
- [5] Y. Yang, K. Vella, and D. P. Holmes, “Grasping with kirigami shells,” *Sci. Robot.*, vol. 6, no. 54, p. eabd6426, 2021.
- [6] Y. Hong, Y. Chi, S. Wu, Y. Li, Y. Zhu, and J. Yin, “Boundary curvature guided programmable shape-morphing kirigami sheets,” *Nat. Commun.*, vol. 13, no. 1, pp. 1–13, 2022.
- [7] J. N. Grima, A. Alderson, and K. E. Evans, “Negative Poisson’s ratios from rotating rectangles,” *Comput. Methods Sci. Technol.*, vol. 10, no. 2, pp. 137–145, 2004.
- [8] H. Mitschke, V. Robins, K. Mecke, and G. E. Schröder-Turk, “Finite auxetic deformations of plane tessellations,” *Proc. R. Soc. A*, vol. 469, no. 2149, p. 20120465, 2013.
- [9] S. Shan, S. H. Kang, Z. Zhao, L. Fang, and K. Bertoldi, “Design of planar isotropic negative Poisson’s ratio structures,” *Extreme Mech. Lett.*, vol. 4, pp. 96–102, 2015.
- [10] B. G.-g. Chen, B. Liu, A. A. Evans, J. Paulose, I. Cohen, V. Vitelli, and C. D. Santangelo, “Topological mechanics of origami and kirigami,” *Phys. Rev. Lett.*, vol. 116, no. 13, p. 135501, 2016.
- [11] A. Rafsanjani and D. Pasini, “Bistable auxetic mechanical metamaterials inspired by ancient geometric motifs,” *Extreme Mech. Lett.*, vol. 9, pp. 291–296, 2016.

- [12] R. M. Neville, F. Scarpa, and A. Pirrera, “Shape morphing kirigami mechanical metamaterials,” *Sci. Rep.*, vol. 6, p. 31067, 2016.
- [13] Y. Tang and J. Yin, “Design of cut unit geometry in hierarchical kirigami-based auxetic metamaterials for high stretchability and compressibility,” *Extreme Mech. Lett.*, vol. 12, pp. 77–85, 2017.
- [14] Y. Tang, G. Lin, S. Yang, Y. K. Yi, R. D. Kamien, and J. Yin, “Programmable kiri-kirigami metamaterials,” *Adv. Mater.*, vol. 29, no. 10, p. 1604262, 2017.
- [15] A. Rafsanjani and K. Bertoldi, “Buckling-induced kirigami,” *Phys. Rev. Lett.*, vol. 118, no. 8, p. 084301, 2017.
- [16] M. Moshe, E. Esposito, S. Shankar, B. Bircan, I. Cohen, D. R. Nelson, and M. J. Bowick, “Kirigami mechanics as stress relief by elastic charges,” *Phys. Rev. Lett.*, vol. 122, no. 4, p. 048001, 2019.
- [17] A. Rafsanjani, L. Jin, B. Deng, and K. Bertoldi, “Propagation of pop ups in kirigami shells,” *Proc. Natl. Acad. Sci.*, vol. 116, no. 17, pp. 8200–8205, 2019.
- [18] L. Liu, G. P. T. Choi, and L. Mahadevan, “Wallpaper group kirigami,” *Proc. R. Soc. A*, vol. 477, no. 2252, p. 20210161, 2021.
- [19] L. Liu, G. P. T. Choi, and L. Mahadevan, “Quasicrystal kirigami,” *Phys. Rev. Research*, 2022.
- [20] N. Singh and M. van Hecke, “Design of pseudo-mechanisms and multistable units for mechanical metamaterials,” *Phys. Rev. Lett.*, vol. 126, no. 24, p. 248002, 2021.
- [21] Y. Zheng, I. Niloy, P. Celli, I. Tobasco, and P. Plucinsky, “Continuum field theory for the deformations of planar kirigami,” *Phys. Rev. Lett.*, vol. 128, p. 208003, 2022.
- [22] M. Czajkowski, C. Coulais, M. van Hecke, and D. Rocklin, “Conformal elasticity of mechanism-based metamaterials,” *Nat. Commun.*, vol. 13, no. 1, pp. 1–9, 2022.
- [23] P. Celli, C. McMahan, B. Ramirez, A. Bauhofer, C. Naify, D. Hofmann, B. Audoly, and C. Daraio, “Shape-morphing architected sheets with non-periodic cut patterns,” *Soft Matter*, vol. 14, no. 48, pp. 9744–9749, 2018.
- [24] M. Konaković-Luković, J. Panetta, K. Crane, and M. Pauly, “Rapid deployment of curved surfaces via programmable auxetics,” *ACM Trans. Graph.*, vol. 37, no. 4, p. 106, 2018.
- [25] G. P. T. Choi, L. H. Dudte, and L. Mahadevan, “Programming shape using kirigami tessellations,” *Nat. Mater.*, vol. 18, no. 9, pp. 999–1004, 2019.
- [26] L. A. Lubbers and M. van Hecke, “Excess floppy modes and multibranching mechanisms in metamaterials with symmetries,” *Phys. Rev. E*, vol. 100, no. 2, p. 021001, 2019.
- [27] C. Jiang, F. Rist, H. Pottmann, and J. Wallner, “Freeform quad-based kirigami,” *ACM Trans. Graph.*, vol. 39, no. 6, pp. 1–11, 2020.
- [28] S. Chen, G. P. T. Choi, and L. Mahadevan, “Deterministic and stochastic control of kirigami topology,” *Proc. Natl. Acad. Sci.*, vol. 117, no. 9, pp. 4511–4517, 2020.
- [29] G. P. T. Choi, L. H. Dudte, and L. Mahadevan, “Compact reconfigurable kirigami,” *Phys. Rev. Research*, vol. 3, no. 4, p. 043030, 2021.
- [30] X. Dang, F. Feng, H. Duan, and J. Wang, “Theorem for the design of deployable kirigami tessellations with different topologies,” *Phys. Rev. E*, vol. 104, p. 055006, 2021.
- [31] L. H. Dudte, G. P. T. Choi, and L. Mahadevan, “An additive algorithm for origami design,” *Proc. Natl. Acad. Sci.*, vol. 118, no. 21, p. e2019241118, 2021.

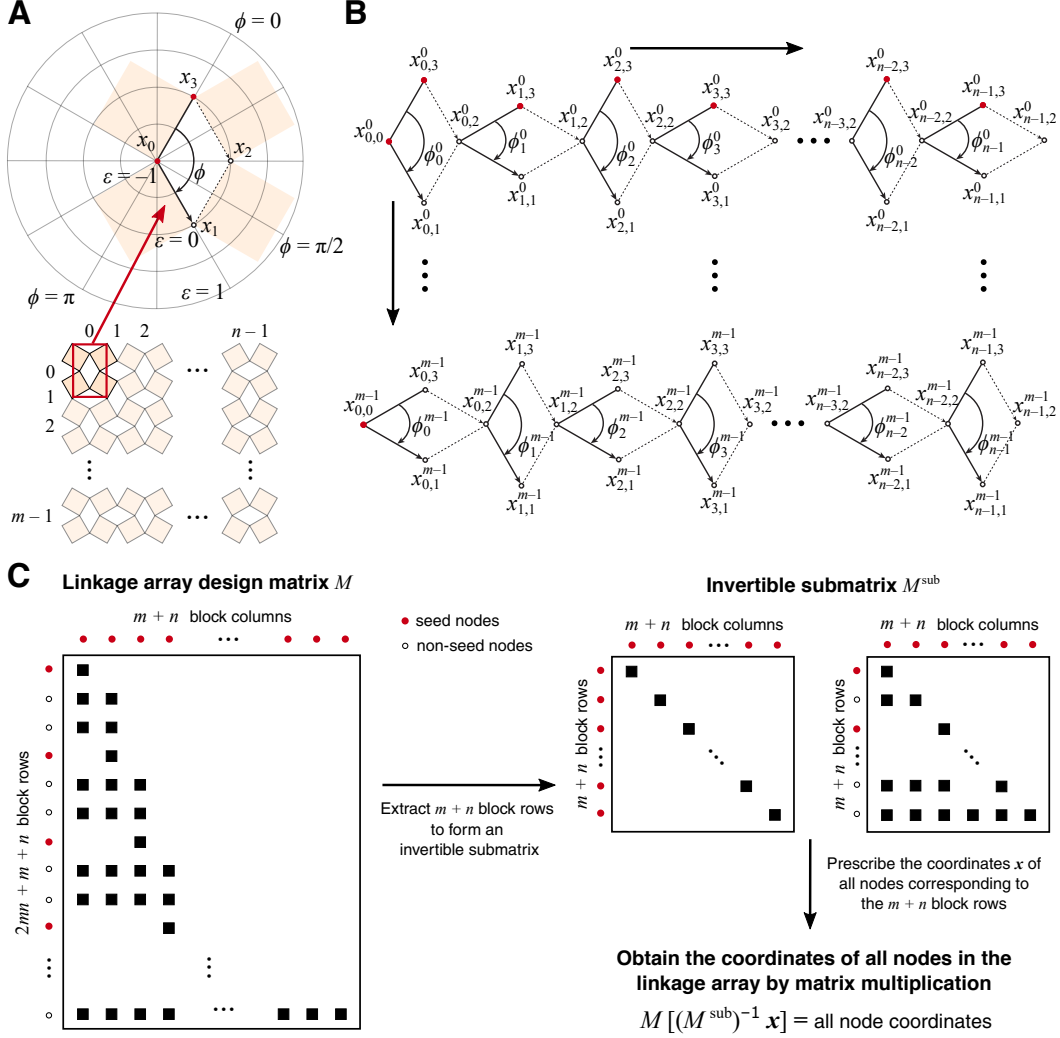


Figure 1: **Marching construction for quad kirigami design.** (A) Geometric design of a four-bar linkage representing a negative space. Given the coordinates of two seed nodes \mathbf{x}_0 and \mathbf{x}_3 (highlighted in red), the linkage can be parameterized by a deployment angle ϕ and an edge length parameter (offset) ϵ . (B) Each linkage strip consists of a series of four-bar linkages each parameterized by ϕ_j and ϵ_j . The coordinates of the non-seed nodes (hollow dots) are dependent of the seed nodes (red dots) as indicated by the arrows in the linkages. One can grow the linkages following the direction of the large arrows to obtain m linkage strips each with n linkages, thereby forming an $m \times n$ linkage array dual to an $(m + 1) \times (n + 1)$ quad kirigami pattern. (C) Considering the relationship between all nodes in the linkage array, we obtain a linkage array design matrix M with all parameters $\{\phi_j^i\}$ and $\{\epsilon_j^i\}$ encoded in it (first panel). Note that M consists of $2mn + m + n$ block rows and $m + n$ block columns, where each block (black square) is a 2×2 matrix corresponding to the xy -coordinates of the each node (see also (3)). One can then extract $m + n$ block rows suitably to form a $(2m + 2n) \times (2m + 2n)$ invertible submatrix M^{sub} . In particular, choosing exactly the $m + n$ block rows corresponding to all seed nodes (red dots) will form an identity matrix $M^{\text{sub}} = I_{2m+2n}$ (second panel, left). Alternatively, one can choose block rows corresponding to some seed nodes (red dots) and some non-seed nodes (hollow dots) to form M^{sub} (second panel, right). In either case, we can then prescribe the coordinates of all nodes corresponding to the chosen $m + n$ block rows, and then invert the submatrix M^{sub} to solve for the seed node coordinates. Finally, by a direct matrix multiplication of M with the solved seed node coordinates, we obtain the entire linkage array.

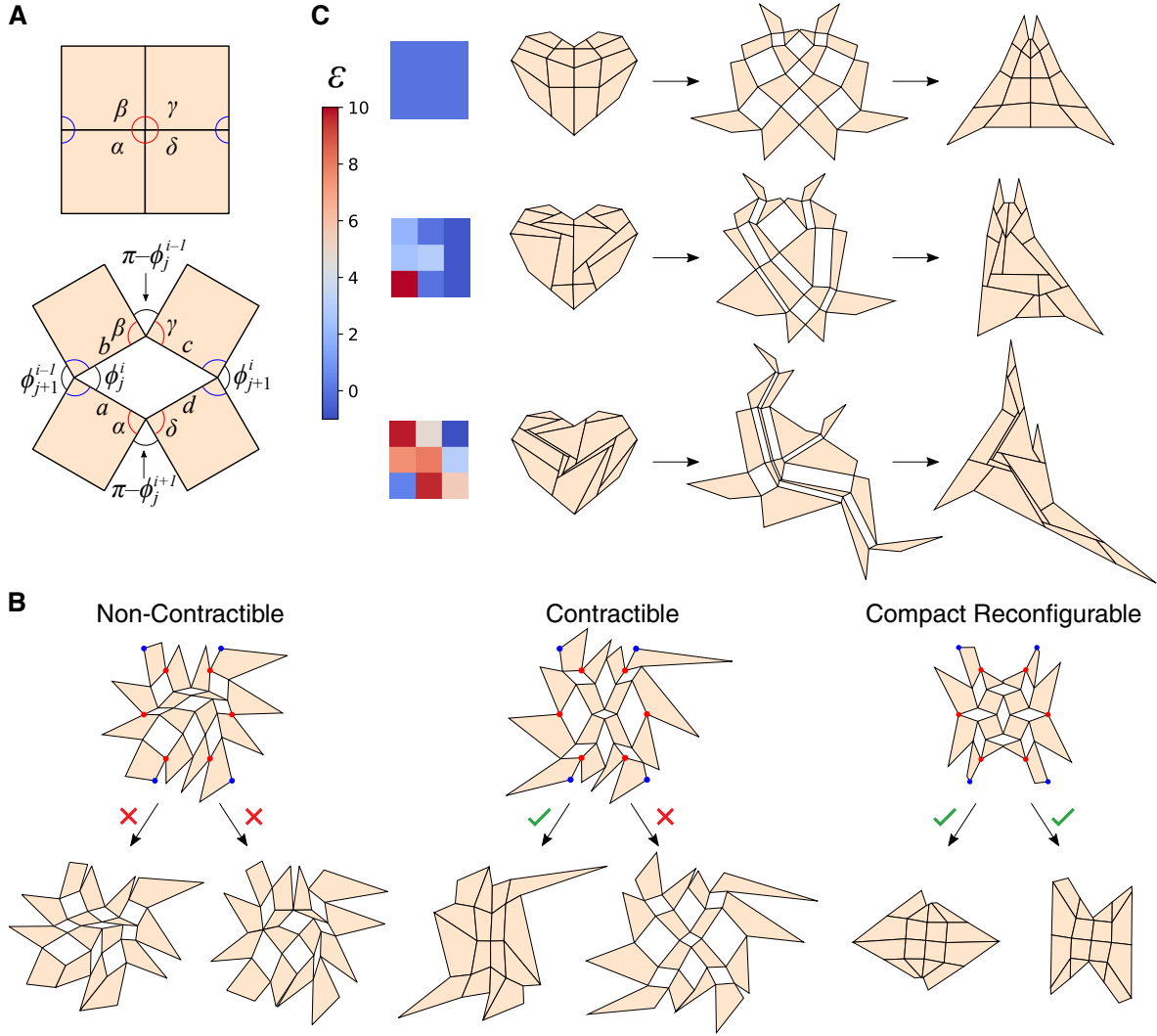


Figure 2: **Encoding different desired properties in the design matrix.** (A) The angle constraints related to contractibility and compact reconfigurability can all be expressed in terms of the deployment angles of adjacent linkages and encoded in the design matrix. The top panel shows a contracted unit cell of four quads. The bottom panel shows a deployed configuration of the unit cell. Note that the four angles highlighted in red determine the contractibility of the unit cell, while the four angles highlighted in blue determine the compact reconfigurability of it. (B) Example choices of the deployment angle field $\{\phi_j^i\}$ that lead to a non-contractible pattern (left), a contractible pattern (middle) and a compact reconfigurable pattern (right). The top row shows three patterns obtained using the proposed design method with a given deployment angle field, where the same linkage boundary node constraints (highlighted in red) and corner constraints (highlighted in blue) are used. In all examples, the offset field $\{\epsilon_j^i\}$ is set to be 0. The bottom row shows the two maximally contracted configurations of each pattern. It can be observed that two closed and compact contracted configurations can be achieved only by using a deployment angle field satisfying the compact reconfigurability condition. (C) Example choices of the offset field $\{\epsilon_j^i\}$. Three compact reconfigurable, rigid-deployable heart shapes are obtained by solving the matrix equation, with the offset at each of 3×3 linkages shown in the corresponding square indicators. As shown by the snapshots of the deployment paths, the offsets yield different interior linkage solutions and influence the deployed geometries, especially the second contracted configurations.

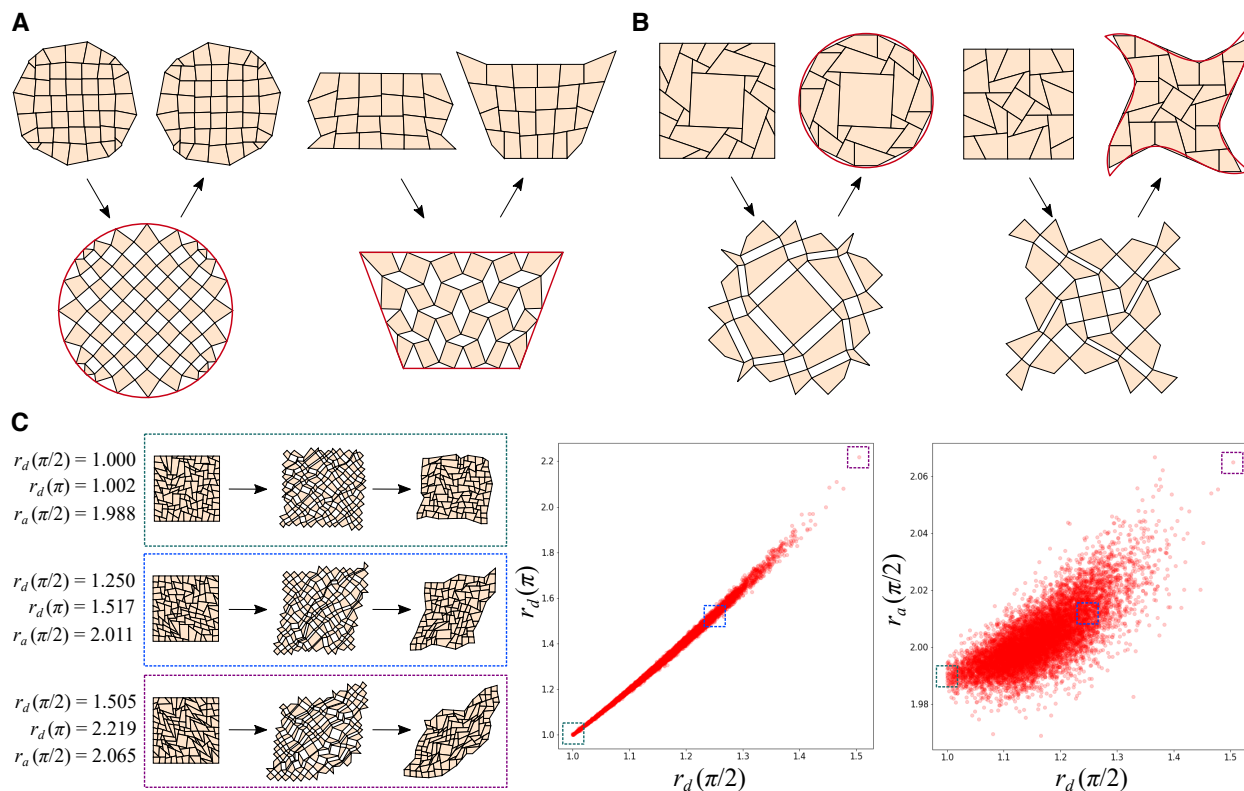


Figure 3: **Linear and nonlinear inverse design of quad kirigami patterns using the proposed framework.** (A) Rigid-deployable, compact reconfigurable kirigami patterns that approximate a target circle and trapezium at two prescribed deployed states $\phi = \pi/2$ and $\phi = \pi/4$ respectively. (B) Patterns that morph from a square to a circle (positive curvature) and a star shape (mixed curvature) in the second contracted state. (C) Statistical analysis of 10000 compact reconfigurable, rigid-deployable square kirigami patterns with random cuts. The left column shows the deployment paths of three random patterns. The middle and right plots show the relationship between the diagonal ratio at the fully deployed state $r_d(\pi/2)$, the diagonal ratio at the second contracted state $r_d(\pi)$ and the maximum deployed area $r_a(\pi/2)$ for all 10000 randomly generated patterns, where each red dot represents a pattern. The positions of the three example patterns on the two scatter plots are boxed.

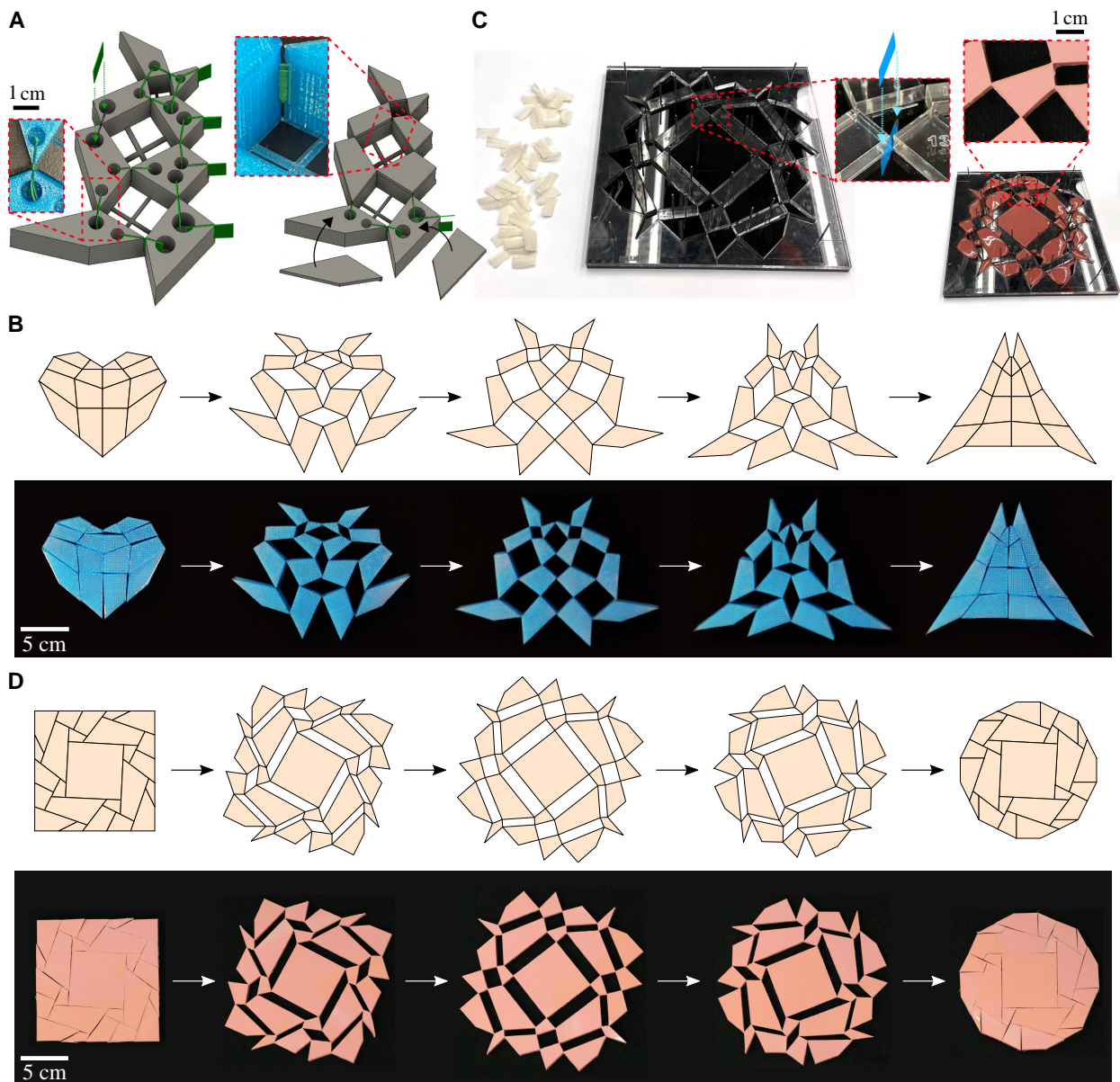


Figure 4: **Physical model fabrication for rigid-deployable kirigami.** (A) A schematic of the 3D-printing based approach. Rigid tiles are first 3D printed, with slots and additional holes created in them. Fabric hinges are then inserted in the slots as indicated by the green arrows, and a set of 3D printed caps are used to cover the holes and form the final structure. (B) Snapshots of the deployment of the heart pattern in Fig. 2C and a corresponding 3D-printed model. (C) A schematic of the casting and molding approach. A 2.5D laser cut mold based on a deployed configuration of a designed pattern is first produced. Fabric pieces are then inserted as indicated by the blue arrows, and the mold is filled with silicone rubber to form the final soft kirigami sheet. (D) Snapshots of the deployment of the square-to-circle pattern in Fig. 3B and a corresponding soft kirigami sheet.